ACS APPLIED MATERIALS & INTERFACES

www.acsami.org

Research Article

Cathode Electrolyte Interphase-Forming Additive for Improving Cycling Performance and Thermal Stability of Ni-Rich $LiNi_xCo_yMn_{1-x-y}O_2$ Cathode Materials

Da-Ae Lim, Young-Kyeong Shin, Jin-Hong Seok, Dayoung Hong, Kyoung Ho Ahn, Chul Haeng Lee, and Dong-Won Kim*

Cite This: *ACS Appl. Mater. Interfaces* 2022, 14, 54688−54697

Read Online

ACCESS | Metrics & More | Article Recommendations | Supporting Information

ABSTRACT: High-capacity Ni-rich $LiNi_xCo_yMn_{1-x-y}O_2$ (NCM) has been investigated as a promising cathode active material for improving the energy density of lithium-ion batteries (LIBs); however, its practical application is limited by its structural instability and low thermal stability. In this study, we synthesized tetrakis(methacryloyloxyethyl)pyrophosphate (TMAEPPi) as a cathode electrolyte interphase (CEI) additive to enhance the cycling characteristics and thermal stability of the $LiNi_{0.8}Co_{0.1}Mn_{0.1}O_2$ (NCM811) material. TMAEPPi was oxidized to form a uniform Li^+-ion-conductive CEI on the cathode surface during initial cycles. A lithium-ion cell (graphite/NCM811) employing a liquid electrolyte containing 0.5 wt % TMAEPPi exhibited superior capacity retention (82.2% after 300 cycles at a 1.0 C rate) and enhanced high-rate performance compared with the cell using a baseline liquid electrolyte. The TMAEPPi-derived CEI layer on NCM811 suppressed electrolyte decomposition and reduced the microcracking of the NCM811 particles. Our results reveal that TMAEPPi is a promising additive for forming stable CEIs and thereby improving the cycling performance and thermal stability of LIBs employing high-capacity NCM cathode materials.

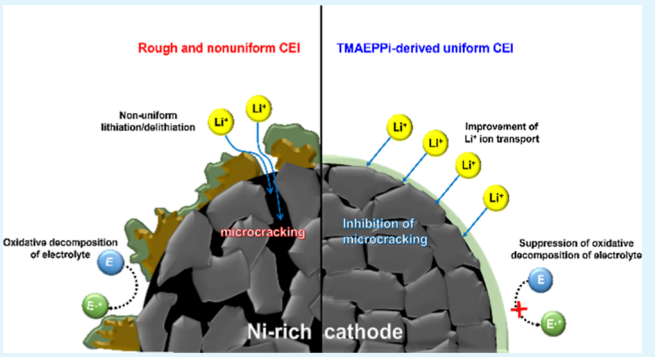

KEYWORDS: *electrolyte additive, cathode electrolyte interphase, nickel-rich cathode, lithium-ion battery, cycling performance, thermal stability.*

INTRODUCTION

High-performance lithium-ion batteries (LIBs) are widely used in mobile electronics as a reliable energy storage source.[1−3] Recently, the interest in eco-friendly policies and energy storage technologies has increased worldwide, and the application fields of LIBs are expanding to large-capacity power sources such as energy storage systems and electric vehicles.[4,5] Accordingly, the demand for LIBs with high energy density, excellent cycle life, and enhanced safety is growing. Because the energy density of LIBs is greatly affected by the operating voltage and capacity of the electrode materials, Ni-rich $LiNi_xCo_yMn_{1-x-y}O_2$ (NCM) materials with high operating voltages and large capacities exceeding 200 mA h g^{-1} have been considered promising cathode materials for LIBs.[6−8] However, these materials have several limitations, such as anodic decomposition of the liquid electrolyte on the cathode derived from highly reactive Ni^{4+}, structural instability caused by microcracking, and safety concerns arising from the low thermal stability of delithiated NCM materials. These problems are more serious at high-voltage operation, resulting in severe degradation of the cell performance upon repeated cycling.[9−13] Therefore, several strategies have been introduced to suppress cell degradation under high-voltage operation, such as active material doping, surface coating, binder modification, morphology control, and design of novel electrolyte systems.[14−24] Among the various approaches, the formation of a uniform and stable cathode electrolyte interphase (CEI) on the cathode active materials by adding an appropriate amount of an additive is an effective way to improve the cycling performance of Ni-rich NCM cathode materials without sacrificing energy density of LIBs. The uniform and stable CEI layer on the NCM surface by the electrochemical reaction of the additive can suppress oxidative decomposition of the liquid electrolyte and maintain the facile intercalation/

Received: August 31, 2022
Accepted: November 22, 2022
Published: December 2, 2022

deintercalation of lithium ions, thereby enhancing the structural stability of the cathode active material.[25−27]

To date, several CEI-forming additives containing polar groups such as P−O, S═O, and C−O have been actively studied.[28,29] The CEI is generally composed of inorganic LiF and organic (carbonate, ether-based polymeric species) components. The resistive LiF component in the CEI layer blocks the migration of lithium ions and thus reduces the reaction kinetics at the cathode side.[30] On the other hand, the polar groups in the CEI layer can improve the Li^+ ion migration by providing a Li^+ ion conduction pathway. Yim et al. reported the improved electrochemical performance of a Li/$LiNi_{0.7}Co_{0.2}Mn_{0.1}O_2$ cell by the addition of divinyl sulfone.[31] Zheng et al. reported the enhanced cycling performance of a Li/$Li_{1.2}Ni_{0.13}Co_{0.13}Mn_{0.54}O_2$ cell by addition of phenyl vinyl sulfone.[32] Recently, Park et al. reported the improved thermal stability and cycling performance of the graphite/$LiNi_{0.8}Co_{0.1}Mn_{0.1}O_2$ (NCM811) cell by adding lithium tetrafluoro(fluoromalonato) phosphate.[33] According to these reports, the polar group is considered a main component of electrolyte additives for forming the CEI layer that improves the electrochemical performance of LIBs.

In the present study, we synthesized tetrakis-(methacryloyloxyethyl)pyrophosphate (TMAEPPi) containing a polar phosphate group because the P−O group in the CEI layer provides a pathway for Li^+ ions and supports to desolvate Li^+ ions from the solvated structure at the cathode surface during the intercalation process. Synthesized TMAEPPi was applied to the lithium-ion cell composed of a graphite anode and NCM811 cathode as a CEI additive to enhance the cycling performance and thermal stability of LIBs. The unique properties of the TMAEPPi-induced CEI that mitigates the degradation of cathode materials and promotes Li^+ ion migration were investigated by X-ray photoelectron spectroscopy (XPS), electrochemical impedance spectroscopy (EIS), transmission electron microscopy (TEM), and scanning electron microscopy (SEM). The effect of TMAEPPi addition on the thermal stability of the cathode was also examined using differential scanning calorimetry (DSC) measurements.

EXPERIMENTAL SECTION

Materials. Diphosphoryl chloride, 2-hydroxyethyl methacrylate, and tetrahydrofuran (THF, anhydrous) were purchased from TCI and used without any treatment. Triethylamine (TEA, anhydrous) and dichloromethane (DCM, anhydrous) were supplied by Sigma-Aldrich and used as received. A polyethylene (PE) separator (9 μm, SK IE Technology Co., Ltd.) was dried under vacuum at 70 °C. The baseline liquid electrolyte was 1.0 M $LiPF_6$ in ethyl methyl carbonate (EMC) and ethylene carbonate (EC) (7:3 by the volume ratio) and was purchased from Dongwha Electrolyte Co. Ltd.

Synthesis of TMAEPPi. TMAEPPi was synthesized via the reaction between diphosphoryl chloride and 2-hydroxyethyl methacrylate. 2-Hydroxyethyl methacrylate (10.0 g), triethylamine (7.78 g), and THF (100 mL) were added to a 250 mL three-neck flask under a dry argon atmosphere. Diphosphoryl chloride (3.22 g) was dropped into the mixed solution at 0 °C using a syringe pump for 1 h, and the reactants were continuously stirred for 48 h at 25 °C. After the reaction was complete, the precipitated salt was removed via filtration. The remaining product was extracted five times with DCM and deionized water. The residual water in the extracted organic layer was removed by adding magnesium sulfate. It was further purified by column chromatography and dried under vacuum at 40 °C. Finally, pure TMAEPPi was obtained as a yellowish oil (4.97 g, yield: 62%). The characterization of TMAEPPi by nuclear magnetic resonance (NMR) spectroscopy was as follows:

^{1}H NMR ($CDCl_3$, 600 MHz, ppm): δ 1.931 (s, 3 H), 4.263−4.301 (m, 2H), 4.332−4.346 (m, 2H), 5.593 (s, 1 H), 6.138 (s, 1H).

^{31}P NMR ($CDCl_3$, 162 MHz, ppm): δ −1.323 (s).

Assembly of the Lithium-Ion Cell. The NCM811 cathode was fabricated from a viscous slurry consisting of 95 wt % NCM811 (L&F Co., Ltd.), 3 wt % poly(vinylidene fluoride) (PVDF, Solef 5130, Solvay), and 2 wt % Super P carbon (TIMCAL) in *N*-methyl pyrrolidone (NMP) on an aluminum current collector. The anode was prepared from a slurry of 91 wt % artificial graphite (S360, BTR), 1 wt % Super P carbon, and 8 wt % PVDF on a copper foil. The mass loading of NCM811 and graphite in the electrodes was 14.0 and 9.8 mg cm^{-2}, respectively. A coin cell was assembled by sandwiching the separator between the graphite anode and the NCM811 cathode. The liquid electrolyte with and without TMAEPPi was then injected into the cell. The content of TMAEPPi added to the baseline electrolyte was in the range of 0.25 to 1.0 wt %. The moisture content in the electrolytes containing TMAEPPi was confirmed to be less than 15 ppm by Karl Fischer (KF) titration. The assembled cells were aged at 30 °C for 24 h prior to the cycling test. All cell assembly procedures were conducted in an Ar-filled glovebox (MBRAUN).

Characterization and Measurements. The highest occupied molecular orbital (HOMO) and lowest unoccupied molecular orbital (LUMO) energy levels of the electrolyte components (solvents, salt, and additive) were obtained by density functional theory (DFT) calculation using Gamess at the B3LYP/6-311++G level. ^{1}H NMR and ^{31}P NMR spectra of the chemicals were obtained in $CDCl_3$ using NMR spectroscopy (VNMRS 600 MHz, Varian). Fourier-transform infrared (FT-IR) spectroscopy of the chemicals was performed between 400 and 4000 cm^{-1} using a Nicolet iS50 spectrometer (Thermo Fisher Scientific Inc). The morphologies of NCM811 cathodes were examined using high-resolution TEM (HR-TEM; JEOL 2100F) and field-emission SEM (FE-SEM; Verios G4). The chemical analysis of the CEI on the NCM811 cathode surface was conducted by XPS (K-Alpha+, Thermo Fisher) with Al Kα as the X-ray source under ultrahigh vacuum. For DSC measurements, the delithiated $Li_{1-x}Ni_{0.8}Co_{0.1}Mn_{0.1}O_2$ cathode was collected and sealed in a Tzero hermetic aluminum pan. Its thermal stability was examined by DSC at a heating rate of 10 °C min^{-1}. The ionic conductivity of the liquid electrolyte was measured using a conductivity meter (Cond 3210, WTW GmbH) as a function of temperature. Linear sweep voltammetry (LSV) was carried out at 1 mV s^{-1} using a CHI 660 analyzer (CH Instruments, Inc.). Cyclic voltammetry (CV) was performed at 0.1 mV s^{-1} on the carbon-coated aluminum working electrode with lithium metal as the reference and counter electrodes. A cycling test of the graphite/NCM811 cell was conducted between 2.5 and 4.3 V using a battery tester (WBCS 3000, WonATech Co. Ltd.) at 25 °C. The cells were subjected to pre-cycling at a 0.1 C rate (two cycles) and 0.2 C rate (three cycles), followed by cycling at a 1.0 C rate to evaluate the cycling stability. At the end of constant current charging, a constant voltage charging was applied to the cell until the current was lower than 0.05 C. To evaluate the rate capability, the cell was charged at the same current rate (0.5 C) and discharged at different current rates: 0.5, 1.0, 2.0, 3.0, and 5.0 C. EIS of the cells before and after cycling was carried out using an impedance analyzer (IM6, Zahner Elektrik) in the frequency range of 10^{-3} to 10^6 Hz at an amplitude of 5 mV.

RESULTS AND DISCUSSION

TMAEPPi was synthesized through a nucleophilic substitution reaction between 2-hydroxyethyl methacrylate and diphosphoryl chloride (Figure S1). Obtained TMAEPPi was characterized using FT-IR, ^{1}H NMR, and ^{31}P NMR spectroscopy. As depicted in Figure S2, the peak of the −OH group in 2-hydroxyethyl methacrylate at 3200 −3600 cm^{-1} disappeared in the TMAEPPi spectrum. The peaks corresponding to the C═C double bonds and C═O groups in TMAEPPi could be observed at 1638 and 1719 cm^{-1}, respectively. The P−Cl peak in diphosphoryl chloride (480−600 cm^{-1}) disappeared, and

https://doi.org/10.1021/acsami.2c15685
ACS Appl. Mater. Interfaces 2022, 14, 54688−54697

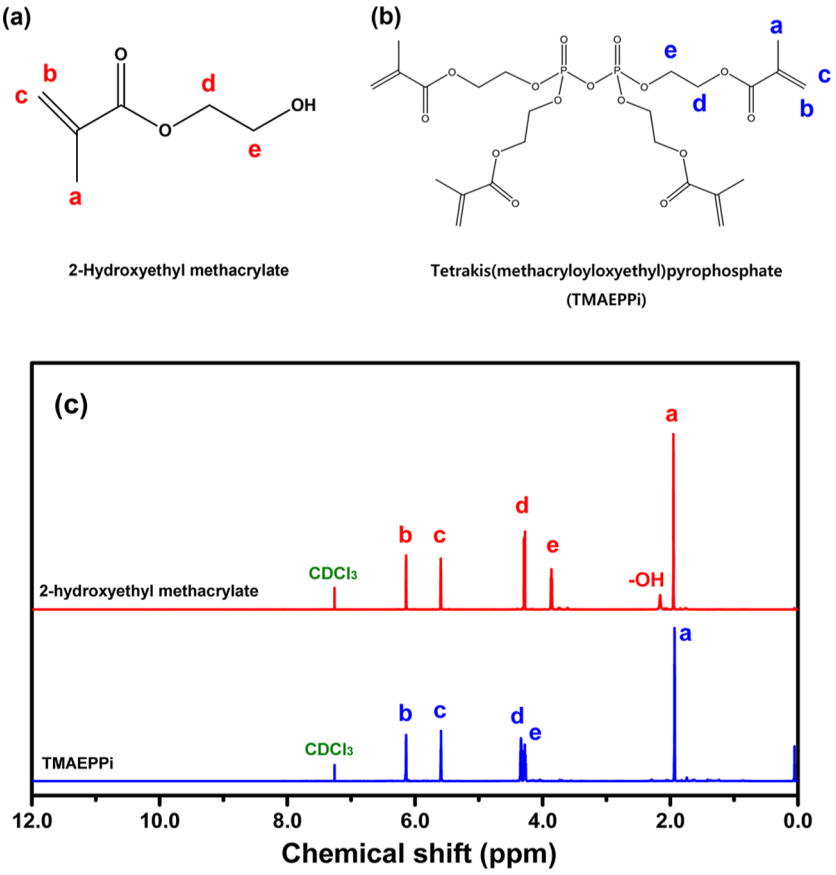

Figure 1. Chemical structures of (a) 2-hydroxyethyl methacrylate and (b) TMAEPPi. (c) ^{1}H NMR spectra of 2-hydroxyethyl methacrylate and TMAEPPi in the $CDCl_3$ solvent.

the new P−O−C peak was observed at 970−1140 cm^{-1} in TMAEPPi after the reaction. Figure 1 shows the ^{1}H NMR spectra of 2-hydroxyethyl methacrylate and TMAEPPi. The peak of −OH in 2-hydroxyethyl methacrylate (δ = 2.15 ppm) completely disappeared in TMAEPPi, and the $-CH_2-$ peak adjacent to −OH shifted from 3.85 to 4.27 ppm after the −OH group was replaced by the −PO group by the substitution reaction. The peak of $-OP(=O)Cl_2$ in diphosphoryl chloride (δ = −9.46 ppm) shifted completely to −1.32 ppm by the replacement of chlorine atoms with oxygen atoms after the reaction, as presented in the ^{31}P NMR spectra of Figure S3. These results suggest that TMAEPPi was successfully synthesized from diphosphoryl chloride and 2-hydroxyethyl methacrylate, without any residual impurities in the product.

Figure 2a presents the LUMO and HOMO energy levels of EC, EMC, $LiPF_6$, and TMAEPPi, which were obtained from DFT calculations. Their optimal molecular structures for DFT calculations are given in Figure S4. As depicted in Figure 2a, the HOMO energy of TMAEPPi is much higher than that of the solvents (EC: −8.38 eV, EMC: −8.05 eV) and lithium salt ($LiPF_6$: −10.77 eV) in the baseline electrolyte. This indicates that TMAEPPi is likely oxidized to form a CEI layer on the cathode surface prior to the oxidative decomposition of the electrolyte components during the charging process. Figure 2b depicts the ionic conductivities of the electrolytes without and with 0.5 wt % TMAEPPI as a function of the temperature. It can be seen that the addition of TMAEPPi has little effect on the ionic conductivity of the liquid electrolyte. CV of the liquid electrolytes without and with TMAEPPi was conducted. As depicted in Figure 2c, no noticeable oxidation peaks were present in the baseline electrolyte. In contrast, an anodic peak was present around 3.9 V *versus* Li/Li^+ in the electrolyte containing 0.5 wt % TMAEPPI (Figure 2d), which can be ascribed to the electrochemical oxidation of TMAEPPI. In subsequent cycles, the anodic current is decreased with cycling in both cells, which implies that a protective layer formed on the electrode surface during the first cycle suppresses the electrolyte decomposition. LSV of the liquid electrolytes was performed to investigate the reductive behavior of TMAEPPi. As shown in Figure S5, no additional reduction peaks due to the addition of TMAEPPI are present, indicating that the additive does not affect the reductive behavior of the electrolyte solution at the anode side during the charge and discharge cycles.

Figure 3a presents the voltage profiles of the graphite/NCM811 cells with different liquid electrolytes during the first formation cycle. The cell employing the baseline electrolyte without TMAEPPi delivered a discharge capacity of 201.0 mA h g^{-1} based on the NCM811 material, with an initial efficiency of 86.3%. In contrast, the cell with 0.5 wt % TMAEPPi showed a lower discharge capacity of 198.6 mA h g^{-1} and a lower efficiency of 82.6%. The lower initial efficiency of the cell with TMAEPPi can be attributed to the irreversible oxidative reaction of TMAEPPi during the first charging process, resulting in the formation of a TMAEPPi-derived CEI on the cathode. After two formation cycles, the cells were further pre-cycled three times at 0.2 C before the long-term cycling test. As presented in Figure S6, both cells delivered almost the same discharge capacities during the three cycles. After pre-cycles, the cells were cycled between 2.5 and 4.3 V at the 1.0 C rate.

https://doi.org/10.1021/acsami.2c15685
ACS Appl. Mater. Interfaces 2022, 14, 54688−54697

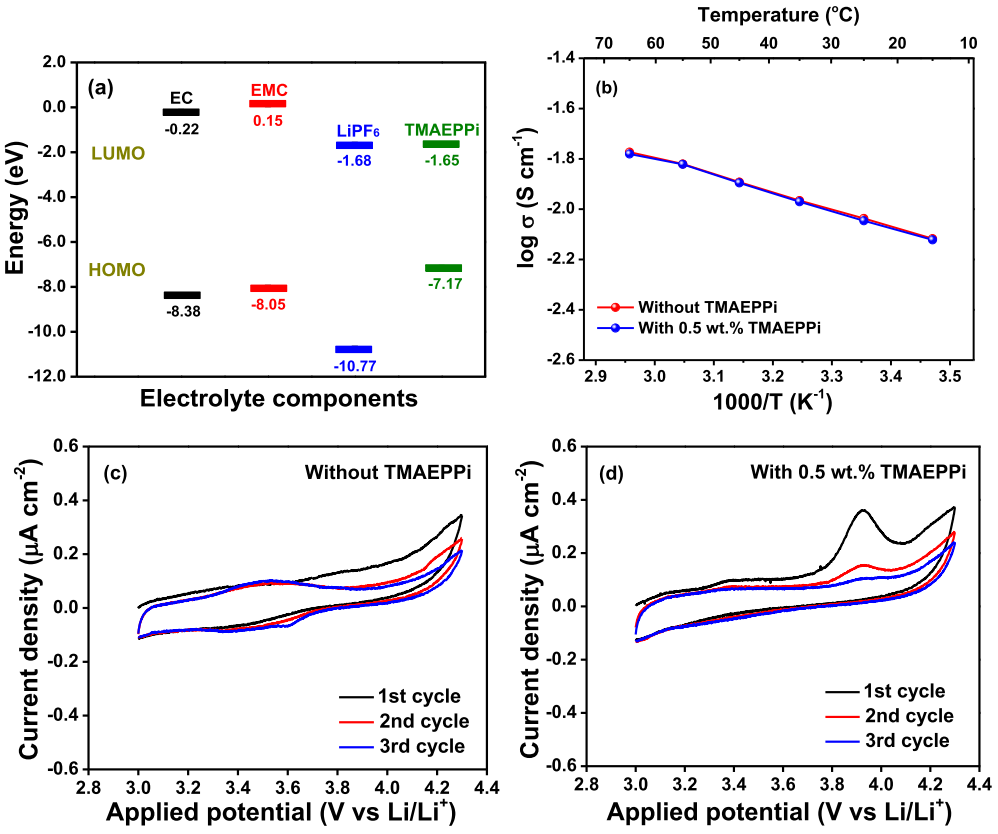

Figure 2. (a) LUMO and HOMO energy levels of organic solvents, salt, and TMAEPPi. (b) Ionic conductivities of liquid electrolytes without and with TMAEPPi as a function of the temperature. Cyclic voltammograms of liquid electrolytes (c) without and (d) with TMAEPPi.

To investigate the effect of the TMAEPPi content on the cycling characteristics of the cell, the cycling performance was compared between the cells containing different contents of TMAEPPi (Figure S7). As depicted in Figure S7e, the cell with 0.5 wt % TMAEPPi showed the best cycling performance. When the TMAEPPi content was less than 0.5 wt %, it was difficult to form a stable CEI on the cathode surface, whereas a high content of TMAEPPI results in the formation of a thick CEI layer with high surface film resistance.[34−36] In order to confirm these presumptions, we obtained the TEM images of NCM811 particles after pre-cycling (Figure S8). When 0.25 wt % TMAEPPi was added, the thin and non-uniform CEI was formed on the NCM811 particle. On the other hand, a thicker CEI layer was produced when adding 0.75 wt % TMAEPPi. From these results, it is concluded that the optimum content of TMAEPPi for achieving good cycling performance is 0.5 wt % in this study. Accordingly, the TMAEPPi content was maintained at 0.5 wt % in the subsequent experiments. The cell employing 0.5 wt % TMAEPPi delivered an initial discharge capacity of 187.0 mA h g^{-1} and exhibited a high capacity retention of 82.2% after 300 cycles at the 1.0 C rate, as presented in Figure 3b,c. The cell showed high cycling efficiencies throughout the cycling after several initial cycles. In contrast, the cell with the baseline electrolyte exhibited greater capacity fading than the cell with TMAEPPi. The enhanced cycling stability in the TMAEPPi-containing cell can be attributed to the presence of a stable CEI layer on the NCM811 surface by the oxidation of TMAEPPi during the initial cycles.

Figure 3d,e presents the EIS results of lithium-ion cells without and with 0.5 wt % TMAEPPi during cycling, showing two overlapping semicircles. As given in the equivalent circuit (Figure S9), the semicircle in the high-frequency region corresponds to the ion transport in the surface film (R_f) formed at the electrode surface, and the semicircle in the mid- to low-frequency region is related to the charge transfer reaction (R_{ct}) at the interface between the electrolyte and electrode.[37] The obtained EIS data were fitted by the equivalent circuit, and the fitting results are given in Table S1. After the first cycle, the total interfacial resistances (R_f + R_{ct}) are similar, irrespective of the presence of TMAEPPi, and then gradually increase with cycling in both cells. It should be noted that the increase in interfacial resistance in the TMAEPPi-containing cell during cycling is relatively small compared to that in the cell without TMAEPPi. Consequently, the cell with TMAEPPi shows a lower interfacial resistance than the cell with the baseline electrolyte after 300 cycles. As discussed earlier, the addition of TMAEPPi induces the formation of the CEI on the cathode surface, which suppresses the oxidative decomposition of the electrolyte and deterioration of the cathode active materials during repeated cycling, thereby mitigating the increase in interfacial resistance in the cell. The leakage current of the cell was measured at 4.3 V after three pre-cycles to investigate the role of the TMAEPPi-derived CEI in the oxidative stability of the electrolyte at the cathode during high-voltage charging.[38,39] As depicted in Figure S10, the cell with 0.5 wt % TMAEPPi showed a lower leakage current than the cell with the baseline electrolyte, which indicates that the CEI layer inhibits the deleterious electrochemical oxidation of the electrolyte at high voltage.

The morphologies of the CEI layer formed on the NCM particle were examined using TEM images obtained before and

https://doi.org/10.1021/acsami.2c15685
ACS Appl. Mater. Interfaces 2022, 14, 54688−54697

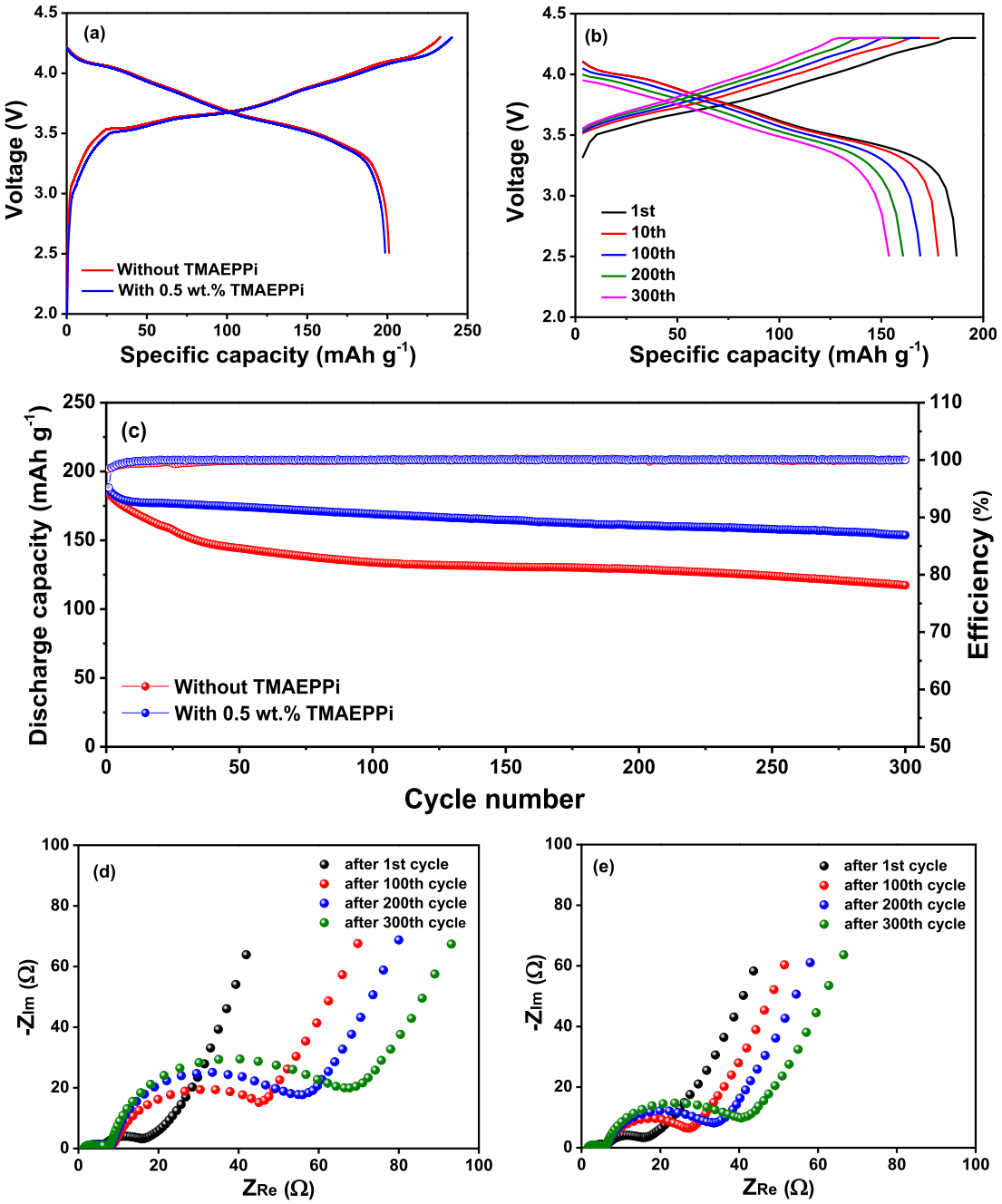

Figure 3. (a) Cycling curves of the lithium-ion cells with different electrolytes for the first formation cycle. (b) Voltage profiles of the cell with the electrolyte containing 0.5 wt % TMAEPPi at 1.0 C. (c) Cycling performance of the cells without and with TMAEPPi at 1.0 C. EIS results of the cells (d) without and (e) with TMAEPPi during cycling.

after three pre-cycles. As depicted in Figure 4b, the cathode particle cycled in the liquid electrolyte without TMAEPPi is covered with a thick and non-uniform surface film with a thickness of 10−20 nm, which arose from the decomposition of the electrolyte components (organic solvents and salt). In contrast, the addition of 0.5 wt % TMAEPPi gives rise to the formation of a thin (~5 nm) and uniform CEI layer (Figure 4c). The cross-sectional morphologies of the cathode were investigated using SEM images recorded before and after 300 cycles, and the results are presented in Figure 4d−f. There was a clear difference in the structural stability of the NCM particles cycled in the electrolytes without and with TMAEPPi. That is, the NCM material cycled without TMAEPPi exhibited intergranular cracking within the particles. The nonuniform layer on the cathode surface (Figure 4b) in the cell without TMAEPPi led to heterogeneity in the delithiation/lithiation degree across the NCM particles during repeated cycling.[40,41] The inhomogeneous delithiation/lithiation process caused anisotropic volume changes and a large strain of secondary particles, thus accelerating the mechanical cracking of the cathode particles.[42,43] Subsequently, the microcracking of the NCM particles provoked electrolyte penetration into the particles; thereafter, undesired electrolyte decomposition occurred on the newly exposed cathode surface, resulting in degradation of the cycling performance with repeated cycling. In contrast, few cracks were observed in the NCM particles

https://doi.org/10.1021/acsami.2c15685
ACS Appl. Mater. Interfaces 2022, 14, 54688−54697

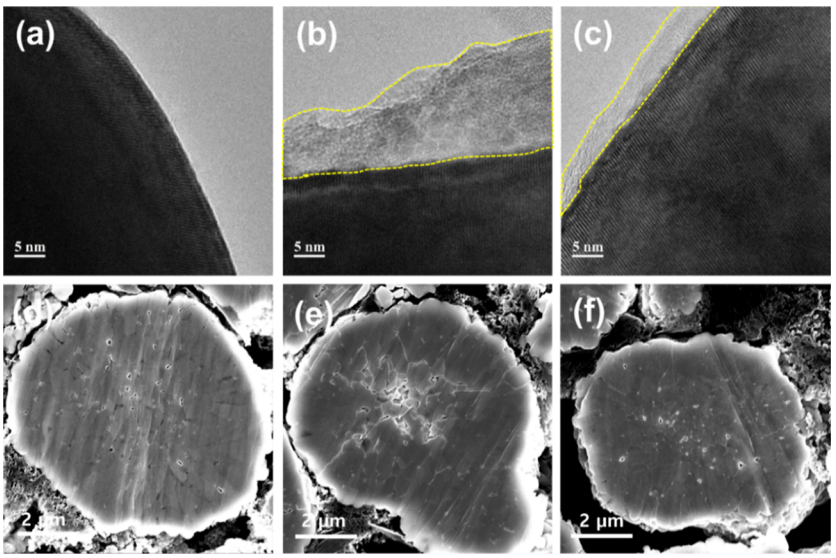

Figure 4. TEM images of NCM811 particles (a) before pre-cycling and after pre-cycling (b) without and (c) with TMAEPPi. Cross-sectional SEM images of the NCM811 particles (d) before and after 300 cycles (e) without and (f) with TMAEPPi.

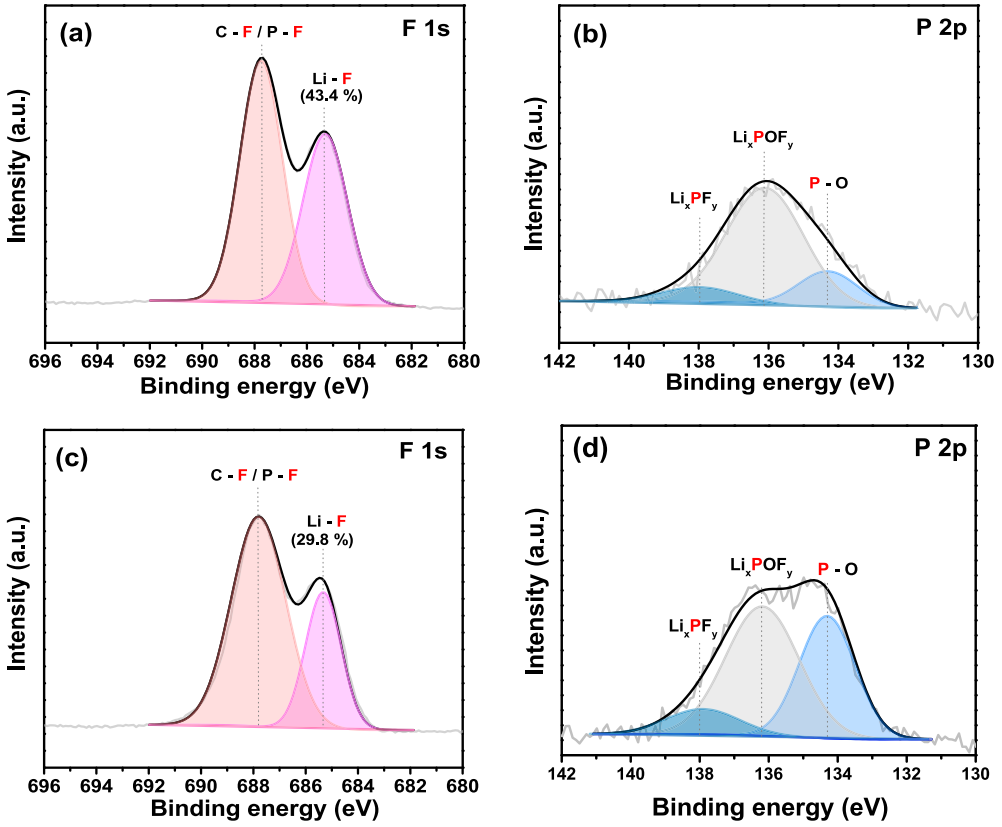

Figure 5. XPS spectra (F 1s and P 2p) of cathodes after three pre-cycles in liquid electrolytes (a,b) without and (c,d) with TMAEPPi.

cycled in the liquid electrolyte containing 0.5 wt % TMAEPPi, which reveals that the addition of TMAEPPi improves the structural and interfacial stability through the uniform and stable CEI layer. Such a difference in the structural stability of the secondary NCM811 particles after repeated cycling was also confirmed from the surface SEM images of the cathodes shown in Figure S11. The surface morphology of the graphite anodes was also examined by SEM analysis. As given in Figure S12, no significant difference is found in the SEM images of the anodes depending on the addition of TMAEPPi, indicating that there is no effect of the additive on the anode side.

The chemical analysis of the CEI layer formed on the cathode was performed using XPS after three pre-cycles in different electrolytes (Figure 5). In the spectra of F 1s (Figure 5a,c), two peaks corresponding to LiF and C−F/P−F are observed at 685.3 and 687.8 eV, respectively.[44−46] The reduced intensity of LiF in the TMAEPPi-containing electrolyte can be attributed to the inhibition of the irreversible decomposition of the electrolyte components by the

https://doi.org/10.1021/acsami.2c15685
ACS Appl. Mater. Interfaces 2022, 14, 54688−54697

TMAEPPi-derived CEI. Because resistive LiF may hinder Li^+ ion transport, a CEI layer with less LiF is desirable. The P 2p spectra in Figure 5b,d show three peaks: phosphate (P−O) at 134.2 eV, Li_xPOF_y (P−O−F) at 136.2 eV, and Li_xPF_y (P−F) at 138.0 eV.[47−49] It is well known that the phosphates in the CEI layer facilitate the migration of lithium ions and promote the charge transfer reaction at the cathode−electrolyte interface.[27] It can be seen that the relative intensity of the phosphate group is significantly increased, and the relative fraction of Li_xPOF_y (P−O−F) generated by hydrofluoric (HF) attack is decreased in the presence of 0.5 wt % TMAEPPi compared to the baseline electrolyte. These results indicate that the improved cycling performance of the TMAEPPi-containing cell is attributed to the presence of the TMAEPPi-derived CEI layer on the cathode surface, which facilitates the cathode kinetics and suppresses the electrolyte decomposition.

The XPS spectra of the anode surface after pre-cycling are given in Figure S13. In the spectra of F 1s, a smaller intensity of LiF is observed when 0.5 wt % TMAEPPi is added due to the suppression of salt decomposition at the cathode side. The relative intensity of phosphate (P−O) in the P 2p spectra is not increased even in the presence of TMAEPPi. These results imply that there is no reaction of TMAEPPi on the anode side.

We investigated the cycling performance of the Li/graphite and Li/NCM811 half-cells with different electrolytes. A cycling test was conducted between 0.005 to 1.5 V and 2.5 to 4.3 V at 0.5 C for Li/graphite and Li/NCM811 cells, respectively. The cells were subjected to pre-cycling at the 0.1 C rate for two cycles, followed by cycling at 0.5 C. As shown in Figure S14, the addition of TMAEPPi hardly affected the cycling characteristics of the Li/graphite cell. On the other hand, the Li/NCM811 cell with 0.5 wt % TMAEPPi exhibited better cycling stability than the cell without TMAEPPi. These results suggest that the improved cycling performance of the graphite/NCM811 cell is related to formation of the CEI on the surface of the NCM811 cathode by addition of TMAEPPi.

The effect of the TMAEPPi addition on the rate performance of the cell was investigated in the cells without and with TMAEPPi. The cells were charged to 4.3 V at the same 0.5 C rate and discharged to 2.5 V at different C rates from 0.5 to 5.0 C. The first discharge curves of the cell with 0.5 wt % TMAEPPi at each C rate are shown in Figure 6a. The increase in the current rate led to a decrease in the cell voltage and discharge capacity owing to the increase in the overpotential. The discharge capacities of the cells without and with TMAEPPi were compared at different C rates. As presented in Figure 6b, the cell with TMAEPPi delivered higher discharge capacities than the cell without TMAEPPi, particularly at high current rates exceeding 2.0 C, indicating that the TMAEPPi-derived CEI improves the migration of Li^+ ions and facilitates the charge transfer reaction, as discussed earlier.

We investigated the cycling performance of the cells without and with TMAEPPi at 55 °C and 1.0 C. As presented in Figure S15, the cell with 0.5 wt % TMAEPPi showed better capacity retention, which can be attributed to suppression of side reactions of the electrolyte with cathode materials at high temperature by the TMAEPPi-derived CEI layer. The thermal stability of the delithiated cathode is an important factor that affects battery safety.[50−52] To investigate the thermal stability of the charged cathodes, the cells were fully charged to 4.3 V at 0.1 C after 300 cycles at 1.0 C and then disassembled to collect the cathode materials in an argon atmosphere. Figure 7 shows

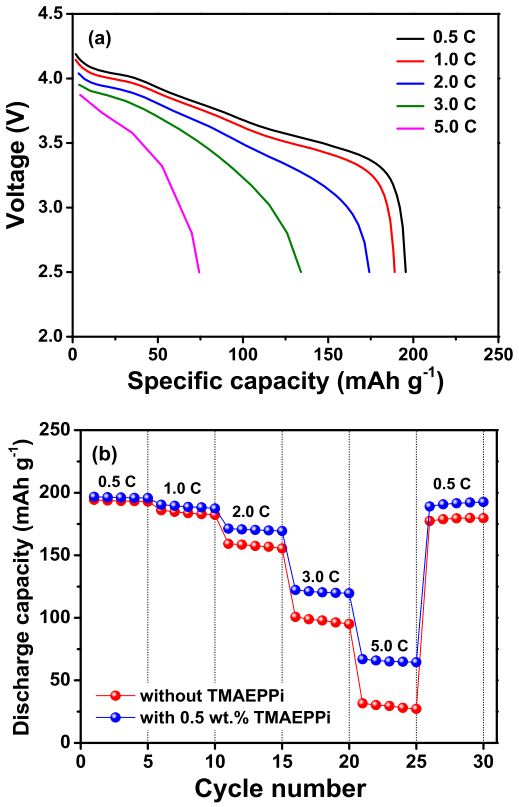

Figure 6. (a) Discharge curves of the cell with 0.5 wt % TMAEPPi at different C rates. (b) Discharge capacities of the cells without and with 0.5 wt % TMAEPPi as a function of the C rate.

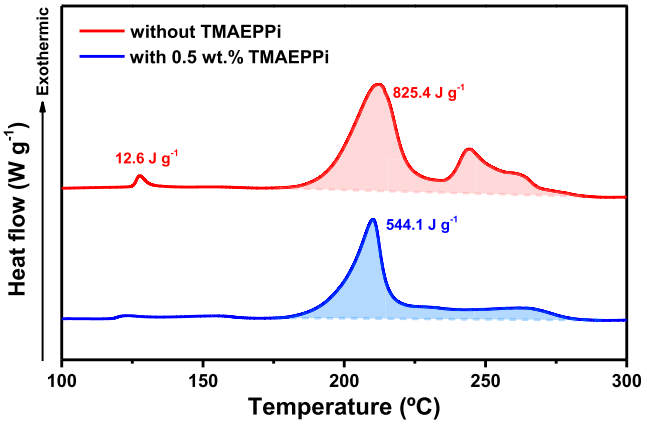

Figure 7. DSC thermograms of delithiated NCM811 cathodes after 300 cycles in the liquid electrolytes without and with 0.5 wt % TMAEPPi.

the DSC thermograms of the delithiated NCM811 cathodes without and with TMAEPPi. The cathode cycled in the baseline electrolyte shows one exothermic peak at approximately 130 °C with a small heat of 12.6 J g^{-1} and two exothermic peaks between 180 and 280 °C with a large heat of 825.4 J g^{-1}. The small exothermic peak at 130 °C can be attributed to the thermal decomposition of the unstable CEI layer, and the exothermic peaks observed at higher temperatures are ascribed to the oxidation between the liquid electrolyte and the oxygen gas released by the structural degradation of delithiated NCM ($Li_{1-x}Ni_{0.8}Co_{0.1}Mn_{0.1}O_2$).[53−56] The amount of heat due to

https://doi.org/10.1021/acsami.2c15685
ACS Appl. Mater. Interfaces 2022, 14, 54688−54697

the exothermic oxidation reaction was reduced to 544.1 J g^{-1} in the cell containing 0.5 wt % TMAEPPi, indicating that the TMAEPPi-derived stable CEI improves the thermal stability of the charged cathode.

Based on the results of this study, the mechanism for enhancing the cycling characteristics and thermal stability of NCM811 materials using the TMAEPPi-derived CEI layer is schematically illustrated in Figure 8. The resistive and nonuniform CEI layer formed in the baseline electrolyte degraded the cycling performance owing to electrolyte decomposition at high voltages, and microcracks occurred within the particles. In contrast, the thin, uniform, and ion-conductive TMAEPPi-based CEI layer facilitated the migration of lithium ions, allowing the uniform deintercalation/intercalation of lithium ions to prevent microcracking in the cathode active material, and reduced the anodic decomposition of the liquid electrolyte during repeated cycling, resulting in improved cycling characteristics and thermal stability of the Ni-rich NCM cathode material.

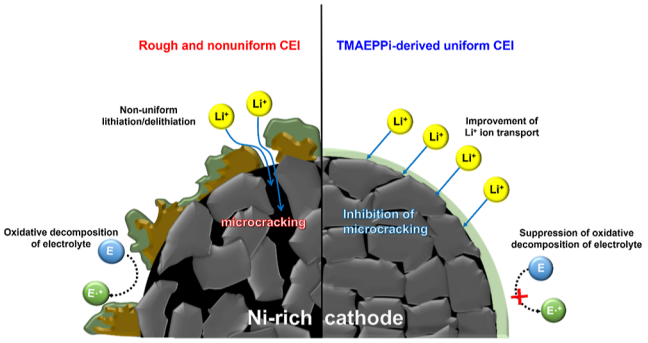

Figure 8. Schematic illustration showing the role of the TMAEPPi-derived CEI formed on the Ni-rich NCM cathode materials.

CONCLUSIONS

TMAEPPi was synthesized and applied as a CEI-forming additive in the LIBs with a high-capacity NCM cathode. TMAEPPi was oxidized on the cathode surface to form a thin and uniform CEI layer prior to anodic decomposition of the solvents and lithium salt. The uniform and ion-conductive TMAEPPi-derived CEI suppressed electrolyte decomposition on the cathode surface at high voltage and thus mitigated the increase in interfacial resistances in the cells. The uniformity of the layer also allowed the homogeneous deintercalation/intercalation of Li^+ ions and enhanced the structural stability of the cathode active materials. Consequently, the addition of 0.5 wt % TMAEPPi to the liquid electrolyte enhanced the cycling performance of the lithium-ion cell in terms of capacity retention and rate performance. Moreover, the TMAEPPi-derived CEI layer improved the thermal stability of delithiated NCM cathode materials. Our results reveal that TMAEPPi is a promising CEI additive for improving the cycling performance and thermal stability of high-capacity Ni-rich Li-$Ni_xCo_yMn_{1-x-y}O_2$ cathode materials.

ASSOCIATED CONTENT

Supporting Information

The Supporting Information is available free of charge at https://pubs.acs.org/doi/10.1021/acsami.2c15685.

Synthesis of TMAEPPi; FT-IR spectra of 2-hydroxyethyl methacrylate, diphosphoryl chloride, and TMAEPPi; ^{31}P NMR spectra of diphosphoryl chloride and TMAEPPi; optimal molecular structures of EC, EMC, $LiPF_6$, and TMAEPPi; linear sweep voltammograms of different electrolytes; cycling curves of the cells without and with TMAEPPi during three pre-cycles at 0.2 C; cycling characteristics of the cells with different contents of TMAEPPi at the 1.0 C rate and 25 °C; TEM images of NCM811 particles after pre-cycling; equivalent circuit for fitting the EIS results; EIS fitting results of the cells during cycling; leakage current of the cells without and with TMAEPPi; SEM images of the cathodes cycled without and with TMAEPPi; SEM images of the anodes without and with TMAEPPi after 300 cycles; XPS spectra of anodes after three pre-cycles without and with TMAEPPi; cycling performance of the Li/graphite and Li/NCM811 half-cells with different electrolytes; and cycling performance of the cells without and with TMAEPPi at 1.0 C and 55 °C (PDF)

AUTHOR INFORMATION

Corresponding Author

Dong-Won Kim − *Department of Chemical Engineering, Hanyang University, Seoul 04763, South Korea;* orcid.org/0000-0002-1735-0272; Phone: +82 2 2220 2337; Email: dongwonkim@hanyang.ac.kr

Authors

Da-Ae Lim − *Department of Chemical Engineering, Hanyang University, Seoul 04763, South Korea*

Young-Kyeong Shin − *Department of Chemical Engineering, Hanyang University, Seoul 04763, South Korea*

Jin-Hong Seok − *Department of Chemical Engineering, Hanyang University, Seoul 04763, South Korea*

Dayoung Hong − *Department of Chemical Engineering, Hanyang University, Seoul 04763, South Korea*

Kyoung Ho Ahn − *Battery R&D, LG Energy Solution, Ltd., Daejeon 34122, South Korea*

Chul Haeng Lee − *Battery R&D, LG Energy Solution, Ltd., Daejeon 34122, South Korea*

Complete contact information is available at: https://pubs.acs.org/10.1021/acsami.2c15685

Notes

The authors declare no competing financial interest.

ACKNOWLEDGMENTS

The authors thank LG Energy Solution and the National Research Foundation of Korea funded by the Korean government (2021R1A2C2011050) for providing the financial support.

REFERENCES

(1) Etacheri, V.; Marom, R.; Elazari, R.; Salitra, G.; Aurbach, D. Challenges in the Development of Advanced Li-Ion Batteries: A Review. *Energy Environ. Sci.* **2011**, *4*, 3243−3262.

(2) Armand, M.; Tarascon, J.-M. Building Better Batteries. *Nature* **2008**, *451*, 652−657.

(3) Goodenough, J. B.; Kim, Y. Challenges for Rechargeable Li Batteries. *Chem. Mater.* **2010**, *22*, 587−603.

(4) Choi, J. W.; Aurbach, D. Promise and Reality of Post-Lithium-Ion Batteries with High Energy Densities. *Nat. Rev. Mater.* **2016**, *1*, 16013.
(5) Cano, Z. P.; Banham, D.; Ye, S.; Hintennach, A.; Lu, J.; Fowler, M.; Chen, Z. Batteries and Fuel Cells for Emerging Electric Vehicle Markets. *Nat. Energy* **2018**, *3*, 279−289.
(6) Myung, S.-T.; Maglia, F.; Park, K.-J.; Yoon, C. S.; Lamp, P.; Kim, S.-J.; Sun, Y.-K. Nickel-Rich Layered Cathode Materials for Automotive Lithium-Ion Batteries: Achievements and Perspectives. *ACS Energy Lett.* **2017**, *2*, 196−223.
(7) Ding, Y.; Mu, D.; Wu, B.; Wang, R.; Zhao, Z.; Wu, F. Recent Progresses on Nickel-Rich Layered Oxide Positive Electrode Materials Used in Lithium-Ion Batteries for Electric Vehicles. *Appl. Energy* **2017**, *195*, 586−599.
(8) Kim, J.-H.; Park, K.-J.; Kim, S. J.; Yoon, C. S.; Sun, Y.-K. A method of increasing the energy density of layered Ni-rich $Li[Ni_{1-2x}Co_xMn_x]O_2$ cathodes (x = 0.05, 0.1, 0.2). *J. Mater. Chem. A* **2019**, *7*, 2694−2701.
(9) Kondo, Y.; Abe, T.; Yamada, Y. Kinetics of Interfacial Ion Transfer in Lithium-Ion Batteries: Mechanism Understanding and Improvement Strategies. *ACS Appl. Mater. Interfaces* **2022**, *14*, 22706−22718.
(10) Ryu, H.-H.; Park, K.-J.; Yoon, C. S.; Sun, Y.-K. Capacity Fading of Ni-Rich $Li[Ni_xCo_yMn_{1-x-y}]O_2$ ($0.6 \leq x \leq 0.95$) Cathodes for High-Energy-Density Lithium-Ion Batteries: Bulk or Surface Degradation? *Chem. Mater.* **2018**, *30*, 1155−1163.
(11) Manthiram, A.; Knight, J. C.; Myung, S.-T.; Oh, S.-M.; Sun, Y.-K. Nickel-Rich and Lithium-Rich Layered Oxide Cathodes: Progress and Perspectives. *Adv. Energy Mater.* **2016**, *6*, 1501010.
(12) Kim, J.; Lee, H.; Cha, H.; Yoon, M.; Park, M.; Cho, J. Prospect and Reality of Ni-Rich Cathode for Commercialization. *Adv. Energy Mater.* **2018**, *8*, 1702028.
(13) Li, T.; Yuan, X.-Z.; Zhang, L.; Song, D.; Shi, K.; Bock, C. Degradation Mechanisms and Mitigation Strategies of Nickel-Rich NMC-Based Lithium-Ion Batteries. *Electrochem. Energy Rev.* **2020**, *3*, 43−80.
(14) Sari, H. M. K.; Li, X. Controllable Cathode-Electrolyte Interface of $Li[Ni_{0.8}Co_{0.1}Mn_{0.1}]O_2$ for Lithium Ion Batteries: A Review. *Adv. Energy Mater.* **2019**, *9*, 1901597.
(15) Zeng, X.; Zhan, C.; Lu, J.; Amine, K. Stabilization of a High-Capacity and High-Power Nickel-Based Cathode for Li-Ion Batteries. *Chem* **2018**, *4*, 690−704.
(16) Kong, F.; Liang, C.; Longo, R. C.; Yeon, D.-H.; Zheng, Y.; Park, J.-H.; Doo, S.-G.; Cho, K. Conflicting Roles of Anion Doping on the Electrochemical Performance of Li-Ion Battery Cathode Materials. *Chem. Mater.* **2016**, *28*, 6942−6952.
(17) He, T.; Lu, Y.; Su, Y.; Bao, L.; Tan, J.; Chen, L.; Zhang, Q.; Li, W.; Chen, S.; Wu, F. Sufficient Utilization of Zirconium Ions to Improve the Structure and Surface Properties of Nickel-Rich Cathode Materials for Lithium-Ion Batteries. *ChemSusChem* **2018**, *11*, 1639−1648.
(18) Han, B.; Key, B.; Lapidus, S. H.; Garcia, J. C.; Iddir, H.; Vaughey, J. T.; Dogan, F. From Coating to Dopant: How the Transition Metal Composition Affects Alumina Coatings on Ni-Rich Cathodes. *ACS Appl. Mater. Interfaces* **2017**, *9*, 41291−41302.
(19) Lee, Y.-S.; Shin, W.-K.; Kannan, A. G.; Koo, S. M.; Kim, D.-W. Improvement of the Cycling Performance and Thermal Stability of Lithium-Ion Cells by Double-Layer Coating of Cathode Materials with Al_2O_3 Nanoparticles and Conductive Polymer. *ACS Appl. Mater. Interfaces* **2015**, *7*, 13944−13951.
(20) Chang, B.; Kim, J.; Cho, Y.; Hwang, I.; Jung, M. S.; Char, K.; Lee, K. T.; Kim, K. J.; Choi, J. W. Highly Elastic Binder for Improved Cyclability of Nickel-Rich Layered Cathode Materials in Lithium-Ion Batteries. *Adv. Energy Mater.* **2020**, *10*, 2001069.
(21) Su, Y.; Chen, G.; Chen, L.; Lu, Y.; Zhang, Q.; Lv, Z.; Li, C.; Li, L.; Liu, N.; Tan, G.; Bao, L.; Chen, S.; Wu, F. High-Rate Structure-Gradient Ni-Rich Cathode Material for Lithium-Ion Batteries. *ACS Appl. Mater. Interfaces* **2019**, *11*, 36697−36704.
(22) Sun, Y.-K.; Myung, S.-T.; Park, B.-C.; Prakash, J.; Belharouak, I.; Amine, K. High-energy cathode material for long-life and safe lithium batteries. *Nat. Mater.* **2009**, *8*, 320−324.
(23) Ma, H.; Hwang, D.; Ahn, Y. J.; Lee, M.-Y.; Kim, S.; Lee, Y.; Lee, S.-M.; Kwak, S. K.; Choi, N.-S. In Situ Interfacial Tuning to Obtain High-Performance Nickel-Rich Cathodes in Lithium Metal Batteries. *ACS Appl. Mater. Interfaces* **2020**, *12*, 29365−29375.
(24) Wang, J.; Yamada, Y.; Sodeyama, K.; Chiang, C. H.; Tateyama, Y.; Yamada, A. Superconcentrated Electrolytes for a High-Voltage Lithium-Ion Battery. *Nat. Commun.* **2016**, *7*, 12032.
(25) Han, J.-G.; Hwang, E.; Kim, Y.; Park, S.; Kim, K.; Roh, D.-H.; Gu, M.; Lee, S.-H.; Kwon, T.-H.; Kim, Y.; Choi, N.-S.; Kim, B.-S. Dual-Functional Electrolyte Additives toward Long-Cycling Lithium-Ion Batteries: Ecofriendly Designed Carbonate Derivatives. *ACS Appl. Mater. Interfaces* **2020**, *12*, 24479−24487.
(26) Li, Y.; Wang, K.; Chen, J.; Zhang, W.; Luo, X.; Hu, Z.; Zhang, Q.; Xing, L.; Li, W. Stabilized High-Voltage Cathodes via an F-Rich and Si-Containing Electrolyte Additive. *ACS Appl. Mater. Interfaces* **2020**, *12*, 28169−28178.
(27) Kim, K.; Ma, H.; Park, S.; Choi, N.-S. Electrolyte-Additive-Driven Interfacial Engineering for High-Capacity Electrodes in Lithium-Ion Batteries: Promise and Challenges. *ACS Energy Lett.* **2020**, *5*, 1537−1553.
(28) Kim, J.; Adiraju, V. A. K.; Rodrigo, N.; Hoffmann, J.; Payne, M.; Lucht, B. L. Lithium Bis(trimethylsilyl) Phosphate as a Novel Bifunctional Additive for High-Voltage $LiNi_{1.5}Mn_{0.5}O_4$/Graphite Lithium-Ion Batteries. *ACS Appl. Mater. Interfaces* **2021**, *13*, 22351−22360.
(29) Han, J.-G.; Park, I.; Cha, J.; Park, S.; Park, S.; Myeong, S.; Cho, W.; Kim, S.-S.; Hong, S. Y.; Cho, J.; Choi, N.-S. Interfacial Architectures Derived by Lithium Difluoro(bisoxalato) Phosphate for Lithium-Rich Cathodes with Superior Cycling Stability and Rate Capability. *ChemElectroChem* **2017**, *4*, 56−65.
(30) Gauthier, M.; Carney, T. J.; Grimaud, A.; Giordano, L.; Pour, N.; Chang, H. H.; Fenning, D. P.; Lux, S. F.; Paschos, O.; Bauer, C.; Maglia, F.; Lupart, S.; Lamp, P.; Shao-Horn, Y. Electrode-Electrolyte Interface in Li-Ion Batteries: Current Understanding and New Insights. *J. Phys. Chem. Lett.* **2015**, *6*, 4653−4672.
(31) Yim, T.; Kang, K. S.; Mun, J.; Lim, S. H.; Woo, S.-G.; Kim, K. J.; Park, M.-S.; Cho, W.; Song, J. H.; Han, Y.-K.; Yu, J.-S.; Kim, Y.-J. Understanding the effects of a multi-functionalized additive on the cathode-electrolyte interfacial stability of Ni-rich materials. *J. Power Sources* **2016**, *302*, 431−438.
(32) Zheng, X.; Wang, X.; Cai, X.; Xing, L.; Xu, M.; Liao, Y.; Li, X.; Li, W. Constructing a Protective Interface Film on Layered Lithium-Rich Cathode Using an Electrolyte Additive with Special Molecule Structure. *ACS Appl. Mater. Interfaces* **2016**, *8*, 30116−30125.
(33) Park, J. W.; Park, D. H.; Go, S.; Nam, D.-H.; Oh, J.; Han, Y.-K.; Lee, H. Malonatophosphate as an SEI- and CEI-forming additive that outperforms malonatoborate for thermally robust lithium-ion batteries. *Energy Storage Mater.* **2022**, *50*, 75−85.
(34) Li, G.; Liao, Y.; Li, Z.; Xu, N.; Lu, Y.; Lan, G.; Sun, G.; Li, W. Constructing a Low-Impedance Interface on a High-Voltage $LiNi_{0.8}Co_{0.1}Mn_{0.1}O_2$ Cathode with 2,4,6-Triphenyl Boroxine as a Film-Forming Electrolyte Additive for Li-Ion Batteries. *ACS Appl. Mater. Interfaces* **2020**, *12*, 37013−37026.
(35) Qian, Y.; Schultz, C.; Niehoff, P.; Schwieters, T.; Nowak, S.; Schappacher, F. M.; Winter, M. Investigations on the Electrochemical Decomposition of the Electrolyte Additive Vinylene Carbonate in Li Metal Half Cells and Lithium Ion Full Cells. *J. Power Sources* **2016**, *332*, 60−71.
(36) Qin, Z.; Hong, B.; Duan, B.; Hong, S.; Chen, Y.; Lai, Y.; Feng, J. Tributyl Borate as a Novel Electrolyte Additive to Improve High Voltage Stability of Lithium Cobalt Oxide in Carbonate-Based Electrolyte. *Electrochim. Acta* **2018**, *276*, 412−416.
(37) Ahn, J. H.; Kim, H.-M.; Lee, Y.-J.; Esken, D.; Dehe, D.; Song, H. A.; Kim, D.-W. Nanostructured Reactive Alumina Particles Coated with Water-Soluble Binder on the Polyethylene Separator for Highly Safe Lithium-Ion Batteries. *J. Power Sources* **2021**, *506*, 230119.

(38) Kim, K.; Kim, Y.; Park, S.; Yang, H. J.; Park, S. J.; Shin, K.; Woo, J.-J.; Kim, S.; Hong, S. Y.; Choi, N.-S. Dual-Function Ethyl 4,4,4-Trifluorobutyrate Additive for High-Performance Ni-Rich Cathodes and Stable Graphite Anodes. *J. Power Sources* **2018**, *396*, 276−287.
(39) Xue, W.; Huang, M.; Li, Y.; Zhu, Y. G.; Gao, R.; Xiao, X.; Zhang, W.; Li, S.; Xu, G.; Yu, Y.; Li, P.; Lopez, J.; Yu, D.; Dong, Y.; Fan, W.; Shi, Z.; Xiong, R.; Sun, C.-J.; Hwang, I.; Lee, W.-K.; Shao-Horn, Y.; Johnson, J. A.; Li, J. Ultra-High-Voltage Ni-Rich Layered Cathodes in Practical Li Metal Batteries Enabled by a Sulfonamide-Based Electrolyte. *Nat. Energy* **2021**, *6*, 495−505.
(40) Kondrakov, A. O.; Schmidt, A.; Xu, J.; Geßwein, H.; Mönig, R.; Hartmann, P.; Sommer, H.; Brezesinski, T.; Janek, J. Anisotropic Lattice Strain and Mechanical Degradation of High- and Low-Nickel NCM Cathode Materials for Li-Ion Batteries. *J. Phys. Chem. C* **2017**, *121*, 3286−3294.
(41) Liu, H.; Wolfman, M.; Karki, K.; Yu, Y.-S.; Stach, E. A.; Cabana, J.; Chapman, K. W.; Chupas, P. J. Intergranular Cracking as a Major Cause of Long-Term Capacity Fading of Layered Cathodes. *Nano Lett.* **2017**, *17*, 3452−3457.
(42) Lee, Y.; Lee, T.; Kim, S.; Lee, J.; Ahn, Y.; Kim, K.; Ma, H.; Park, G.; Lee, S.-M.; Kwak, S.; Choi, N.-S. Fluorine-incorporated Interface Enhances Cycling Stability of Lithium Metal Batteries with Ni-rich NCM Cathodes. *Nano Energy* **2020**, *67*, 104309.
(43) Ruan, Y.; Song, X.; Fu, Y.; Song, C.; Battaglia, V. Structural evolution and capacity degradation mechanism of $Li-Ni_{0.6}Mn_{0.2}Co_{0.2}O_2$ cathode materials. *J. Power Sources* **2018**, *400*, 539−548.
(44) Hekmatfar, M.; Kazzazi, A.; Eshetu, G. G.; Hasa, I.; Passerini, S. Understanding the Electrode/Electrolyte Interface Layer on the Li-Rich Nickel Manganese Cobalt Layered Oxide Cathode by XPS. *ACS Appl. Mater. Interfaces* **2019**, *11*, 43166−43179.
(45) Liu, Q.; Yang, G.; Li, S.; Zhang, S.; Chen, R.; Wang, Z.; Chen, L. Synergy Effect of Trimethyl Borate on Protecting High-Voltage Cathode Materials in Dual-Additive Electrolytes. *ACS Appl. Mater. Interfaces* **2021**, *13*, 21459−21466.
(46) Kim, J.; Pham, H. Q.; Chung, G. J.; Hwang, E.-H.; Kwon, Y.-G.; Song, S.-W. Impacts of Fluorinated Phosphate Additive on Interface Stabilization of 4.6 V Battery Cathode. *Electrochim. Acta* **2021**, *367*, 137527.
(47) Song, Y.-M.; Kim, C.-K.; Kim, K.-E.; Hong, S. Y.; Choi, N.-S. Exploiting chemically and electrochemically reactive phosphite derivatives for high-voltage spinel $LiNi_{0.5}Mn_{1.5}O_4$ cathodes. *J. Power Sources* **2016**, *302*, 22−30.
(48) Cha, J.; Han, J.-G.; Hwang, J.; Cho, J.; Choi, N.-S. Mechanisms for Electrochemical Performance Enhancement by the Salt-Type Electrolyte Additive, Lithium Difluoro(Oxalato)Borate, in High-Voltage Lithium-Ion Batteries. *J. Power Sources* **2017**, *357*, 97−106.
(49) Wang, J.; Zhao, D.; Cong, Y.; Zhang, N.; Wang, P.; Fu, X.; Cui, X. Analyzing the Mechanism of Functional Groups in Phosphate Additives on the Interface of $LiNi_{0.8}Co_{0.15}Al_{0.05}O_2$ Cathode Materials. *ACS Appl. Mater. Interfaces* **2021**, *13*, 16939−16951.
(50) Wang, Y.; Ren, D.; Feng, X.; Wang, L.; Ouyang, M. Thermal kinetics comparison of delithiated $Li[Ni\ Co\ Mn]O_2$ cathodes. *J. Power Sources* **2021**, *514*, 230582.
(51) Bak, S.-M.; Hu, E.; Zhou, Y.; Yu, X.; Senanayake, S. D.; Cho, S.-J.; Kim, K.-B.; Chung, K. Y.; Yang, X.-Q.; Nam, K.-W. Structural Changes and Thermal Stability of Charged $LiNi_xMn_yCo_zO_2$ Cathode Materials Studied by Combined In Situ Time-Resolved XRD and Mass Spectroscopy. *ACS Appl. Mater. Interfaces* **2014**, *6*, 22594−22601.
(52) Gomez-Martin, A.; Reissig, F.; Frankenstein, L.; Heidbüchel, M.; Winter, M.; Placke, T.; Schmuch, R. Magnesium Substitution in Ni-Rich NMC Layered Cathodes for High-Energy Lithium Ion Batteries. *Adv. Energy Mater.* **2022**, *12*, 2103045.
(53) Hou, J.; Yang, M.; Wang, D.; Zhang, J. Fundamentals and Challenges of Lithium Ion Batteries at Temperatures between −40 and 60 °C. *Adv. Energy Mater.* **2020**, *10*, 1904152.
(54) Zhang, L.; Ma, Y.; Cheng, X.; Zuo, P.; Cui, Y.; Guan, T.; Du, C.; Gao, Y.; Yin, G. Enhancement of high voltage cycling performance and thermal stability of $LiNi_{1/3}Co_{1/3}Mn_{1/3}O_2$ cathode by use of boron-based additives. *Solid State Ionics* **2014**, *263*, 146−151.
(55) Hou, J.; Feng, X.; Wang, L.; Liu, X.; Ohma, A.; Lu, L.; Ren, D.; Huang, W.; Li, Y.; Yi, M.; Wang, Y.; Ren, J.; Meng, Z.; Chu, Z.; Xu, G.-L.; Amine, K.; He, X.; Wang, H.; Nitta, Y.; Ouyang, M. Unlocking the Self-Supported Thermal Runaway of High-Energy Lithium-Ion Batteries. *Energy Storage Mater.* **2021**, *39*, 395−402.
(56) Pang, P.; Tan, X.; Wang, Z.; Cai, Z.; Nan, J.; Xing, Z.; Li, H. Crack-free single-crystal $LiNi_{0.83}Co_{0.10}Mn_{0.07}O_2$ as cycling/thermal stable cathode materials for high-voltage lithium-ion batteries. *Electrochim. Acta* **2021**, *365*, 137380.

https://doi.org/10.1021/acsami.2c15685
ACS Appl. Mater. Interfaces 2022, 14, 54688−54697